J. Fluid Mech. (2001), *vol.* 434, *pp.* 167–180. Printed in the United Kingdom

The constant-V vortex

By ALAN J. FALLER

78 Bellevue Avenue, Melrose, MA 02176, USA
e-mail: afaller@mit.edu

(Received 21 April 2000 and in revised form 28 October 2000)

It has been found that the generation of swirl by a continuous rotary oscillation of a right-circular cylinder partially filled with water can leave a vortex with a radially constant tangential velocity, V, i.e. $\partial V/\partial r = 0$, excepting a small central core and the sidewall boundary layer. This vortex maintains $\partial V/\partial r = 0$ during viscous decay by the turbulent bottom boundary layer, a fact that suggests that $\partial V/\partial r = 0$ is a stable condition for a decaying vortex.

Theory shows that such a profile of V and its steady decay is possible only if the radial transport per unit length in the turbulent Bödewadt boundary layer is $T_{B,t} = AVr/2$ where $A \approx 0.072$ is a dimensionless constant found from the experiment. This model of turbulent transport is extended to a case with $\partial V/\partial r \neq 0$ by an analysis of vortex decay in an experiment started from solid rotation. For this case an additional term proportional to $\partial V/\partial r$ is added to the transport equation.

1. Introduction

As first described by Prandtl (1949) the rotary oscillation of a right-circular cylinder partially filled with liquid produces a rotary wave, and when this wave becomes large enough to be turbulent, it generates a vortex in the main body of the liquid by a conversion of wave angular momentum to vortex angular momentum. The process of rotary oscillation is hereafter referred to as 'rotillation' and is described by figure 1 where the cylinder with centre at C and radius R is rotillated about point O at frequency σ while the vector CR retains a fixed orientation. Thus while the centre C rotates about the origin O with the rotillation radius $r_o = OC$, the cylinder does not rotate on its own axis.

In experiments by this author, when rotillation with continuous wave breaking (spilling) was stopped, the resultant vortex had a tangential speed, $V(r)$, that was independent of radius, r, throughout the main body of the water. Moreover, the condition $\partial V/\partial r = 0$ was maintained during decay of the vortex. It will be shown that $\partial(\partial V/\partial r)/\partial t = 0$ requires a specific condition on the inward radial transport in the turbulent Bödewadt boundary layer beneath the vortex.

An ideal Bödewadt layer (Bödewadt 1941) is the laminar boundary layer beneath a constant-angular-velocity vortex ($\partial\omega/\partial r = 0$) over a smooth stationary boundary. A numerical solution due to A. C. Browning may be found in Schlichting (1960). By analogy with use of the term 'Ekman layer' for diverse situations in rotating systems, the term 'Bödewadt layer' is extended here to vortices with turbulent boundary layers and those with $\partial\omega/\partial r \neq 0$.

A rotillation vortex was generated in water $H = 20\,\text{cm}$ deep, with $R = 7\,\text{cm}$, $\sigma = 17.07\,\text{s}^{-1}$ and $r_o = 0.20\,\text{cm}$. Figure 2 shows a streak photograph 10 s after the

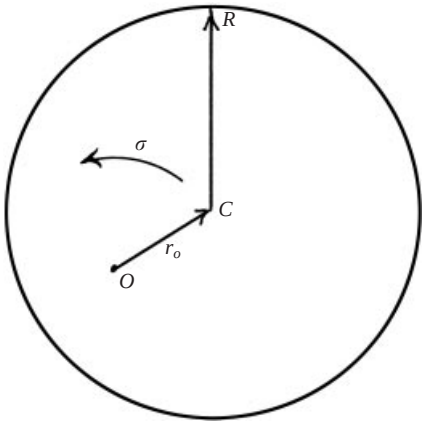

FIGURE 1. Rotillation: a right-circular cylinder of radius R and centre C undergoes a rotary oscillation at frequency σ about an origin O at distance r_o from C. During rotillation the vector CR retains a fixed orientation.

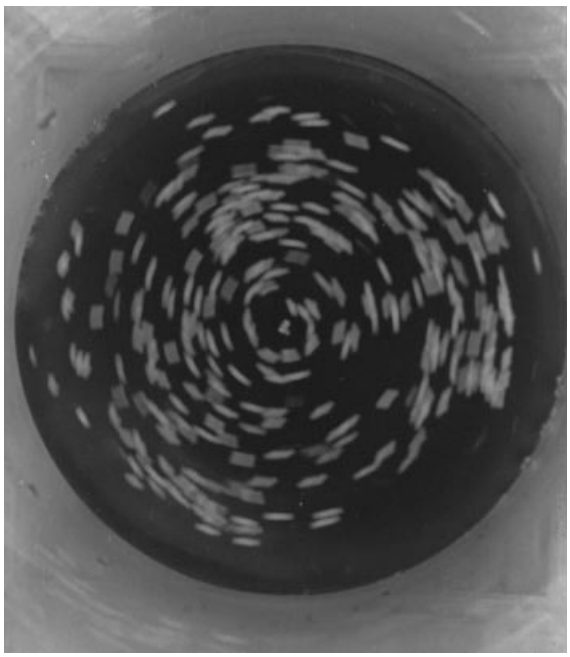

FIGURE 2. A streak photograph 10 s after the cessation of rotillation.

stop of rotillation (which had continued for more than a minute) and clearly gives the impression of a constant streak length. Streak measurements in the interval $2.2 < r < 5.5$ cm at 10, 20 and 30 s (figure 3) gave average speeds of 9.56, 8.53, and 6.83 cm s^{-1}, respectively, with no obvious trend of V with r. At large r the rim boundary layer was centrifugally unstable and thus caused a wide turbulent boundary layer. Near the centre, lateral viscous effects were important, so data in these regions have been omitted. From figure 3 it is assumed that the vortex started with $\partial V/\partial r = 0$ and this state continued during decay. Other experiments with somewhat different σ, R and r_o showed the same characteristic.

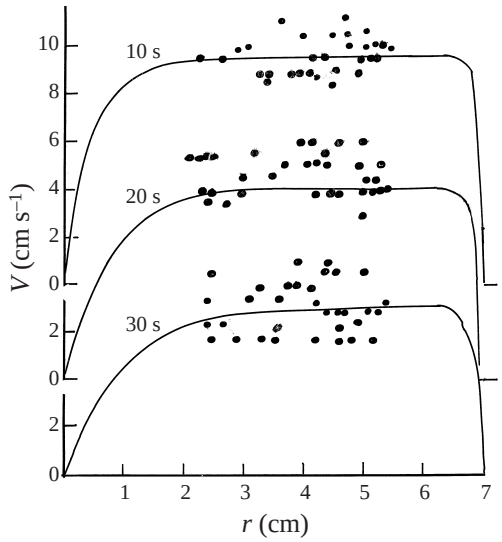

FIGURE 3. Measurements of V at 10, 20 and 30 s after an abrupt stop to rotillation. Beyond 5.5 cm the streaks were erratic because of side boundary-layer turbulence. The curves are from a numerical simulation fit to the data. Note the offset of the ordinate scales to avoid data overlap.

2. Simple models of vortex decay

To motivate a theoretical model of decay for a constant-V vortex it is useful first to review vortex decay for some simple laminar cases. For a vortex with a laminar Ekman or Bödewadt boundary layer it is possible to determine the rate of decay of the vortex from rather simple dynamical arguments. It is then shown that, conversely, by observing the rate of decay of a vortex one can determine the radial boundary-layer transport even for turbulent boundary layers.

2.1. *Spin down with a laminar Ekman layer*

Consider a vortex of constant relative angular velocity ω in a system rotating with a basic angular velocity Ω, $\omega \ll \Omega$. Other conditions of the theory are circular symmetry, $H \gg D_E$, $\partial H/\partial r = 0$, and the neglect of lateral viscous forces in the interior. Here $D_E = (\nu/\Omega)^{1/2}$ is the characteristic depth of a laminar Ekman layer, H is the fluid depth, and ν is the kinematic viscosity. Elementary spin-down theory for $\omega(t)$ involves: (i) the radial Ekman boundary-layer transport, T_E, (ii) continuity, and (iii) the conservation of angular momentum, M, for fluid above the bottom boundary layer. We ignore initial transients during the formation of the boundary layer. Thereafter, for $H \gg D_E$ the boundary-layer transients are negligible and the Ekman boundary-layer transport (radially inward) per unit length of circumference is simply

$$T_E = V D_E/2. \tag{1}$$

By continuity T_E must be balanced by a radially outward interior transport, T_i, which for interior radial speed U is

$$T_i = UH, \tag{2}$$

and so in the interior

$$U = \mathrm{d}r/\mathrm{d}t = V D_E/2H. \tag{3}$$

The angular momentum per unit mass for an interior parcel of fluid is

$$M = (\Omega + \omega)r^2, \tag{4}$$

and by conservation of $M(\mathrm{d}M/\mathrm{d}t = 0)$, with $\omega \ll \Omega$, expansion of $\mathrm{d}\omega/\mathrm{d}t$, and taking $\partial\omega/\partial r = 0$, one finds

$$0 = \partial\omega/\partial t + (\omega\Omega\, D_E/H) \tag{5}$$

with the solution

$$\omega = \omega_o \exp(-t/t_s), \tag{6}$$

where $t_s = H/\Omega D_E$ is the characteristic spin-down time of the vortex and subscript o denotes an initial value. This result was first given by Stern (1960) and later, with a more complete analysis of the transient boundary layer, by Greenspan & Howard (1963). Maas (1993) has considered the effects of the shape of the free surface on the decay of similar vortices but for simplicity the assumption is made here that H is a constant in all cases to be considered.

2.2. *Spin down with a laminar Bödewadt layer*

The key difference between the Ekman and Bödewadt cases is that in the latter $\Omega = 0$. Then as the vortex decays, the boundary-layer depth, $D_B = (\nu/\omega)^{1/2}$, increases. By analogy with (1) the laminar Bödewadt transport may be written as

$$T_B = CV\, D_B/2, \tag{7}$$

where, from a direct numerical integration of the Bödewadt layer, $C = 1.3485$. Then in analogy with (3),

$$U = \mathrm{d}r/\mathrm{d}t = CV\, D_B/2H. \tag{8}$$

By following the same procedure as in § 2.1, the solution is

$$\omega/\omega_o = (1 + C(t/H)(\omega_o\nu)^{1/2})^{-2}, \tag{9}$$

so at large t, ω decays as t^{-2} rather than exponentially as for the Ekman problem. Equation (9) has been confirmed by a numerical integration of spin down with a well-resolved laminar Bödewadt layer.

In a numerical study Faller (1991) found that the Bödewadt layer is first unstable at a critical Reynolds number of $Re_c \approx 15$, where $Re = V\, D_B/\nu = (V\, r/\nu)^{1/2} = r/D_B$. With rather different numerical methods Pikhtov & Smirnov (1992) found $Re_c = 18.8$ and for absolute instability Lingwood (1997) found $Re_c = 21.2$. These very low values, by comparison with $Re_c = 55$ for the Ekman layer, are due primarily to radial convergence and upward flux out of the Bödewadt layer. Savas (1987) has shown experimental evidence of the instability and estimated $Re_c = 25$. Since several issues remain in the question of Bödewadt layer instability a more complete discussion is deferred to a separate communication now in preparation.

In the laboratory experiment of figure 2, Re_c would occur for $r < 0.5$ cm, so except for a very small laminar central core the bottom boundary layer was unstable and we refer to it as being turbulent. Note also that the boundary layer flow convects turbulence inward toward smaller Re, so that at any r the turbulence is augmented by a flux from larger r.

2.3. *The constant-V vortex*

For this analysis start with the angular momentum as $M = Vr$, so the conservation of M is directly

$$V\,\mathrm{d}r/\mathrm{d}t + r\,\mathrm{d}V/\mathrm{d}t = 0, \tag{10}$$

and assume that $\partial V/\partial r = 0$ at all times. Following similar procedures as above one finds

$$\partial V/\partial t = -V^2 C^* D_B/(2Hr), \tag{11}$$

where C is replaced by $C^*(r)$ and where now $D_B = (\nu/\omega)^{1/2} = (\nu r/V)^{1/2}$ is also a function of r. But because the condition $\partial V/\partial r = 0$ is maintained during decay, i.e. $\partial(\partial V/\partial t)/\partial r = 0$, the right-hand side of (11) must be independent of r. Thus, taking $\partial(\,)/\partial r$ of (11) gives

$$0 = (V^2/2H)\,\partial(C^* D_B/r)/\partial r \tag{12}$$

and therefore

$$C^* = A\,r/D_B = AV\,D_B/\nu = ARe. \tag{13}$$

In (13) A is an undetermined dimensionless constant and the Reynolds number is $Re = VD_B/\nu = (Vr/\nu)^{1/2}$. Accordingly, (11) reduces to

$$\partial V/\partial t = -A\,V^2/2H \tag{14}$$

with the solution

$$V/V_o = (1 + AV_0\,t/2H)^{-1}, \tag{15}$$

and at large t, V decays as t^{-1}. The turbulent radial transport now is given by

$$T_{B,t} = AReV\,D_B/2 = AV\,r/2. \tag{16}$$

Thus for a constant-V vortex the rate of vortex decay and the boundary-layer transport are uniquely determined by (15) and (16), respectively. These results have been verified with a numerical model of the decay of a vortex initially having $\partial V/\partial r = 0$ and in which the radial boundary layer flow was parameterized using (16). By fitting this model to the data of figure 3 and minimizing the root-mean-square error (Erms) with A and the unknown V_o as variates, A was found to be $A = 0.072$ with $V_o = 12.0\,\mathrm{cm\,s^{-1}}$.

The computed curves of $V(r)$ at 10, 20, and 30 s are shown in figure 3 for comparison with the data. This numerical model included lateral viscous terms for the interior flow (see §§ 4 and 5), and the term $\nu\,\partial(V/r)/\partial r$ in the Navier–Stokes equation was primarily responsible for the strong decrease of V within $r = 2.5$ cm. A slight viscous effect at larger r also may be seen in the curves of figure 3 as t progresses from 10 to 30 s, and the same effect can be imagined in the data. But because this viscous term is proportional to V/r^2 it would be negligible in larger vortices. Computations without the viscous terms gave $\partial V/\partial r = 0$ at all radii as decay progressed (§ 5).

3. The shape of the free surface

The radial variation of the free surface height, h, in a constant-V vortex is given by

$$h(r) = h(R) - (V^2/g)\,\ln(R/r). \tag{17}$$

In figure 4 this profile is compared with a frame from a 16 mm ciné film for a particularly violent rotillation experiment with $R = 7$ cm, $H = 20$ cm, $r_o = 0.20$ cm and $\sigma = 23.27\,\mathrm{s^{-1}}$. Thus the only difference between this case and that of figure 2 is the frequency, σ. The figure shows a single frame from this turbulent case when the rotillation wave had its crest on the right of the scene and its trough on the left. The approximate intersection of the free surface of the vortex with the cylinder wall is shown by the line sloping upward from the trough on the left to the crest on the

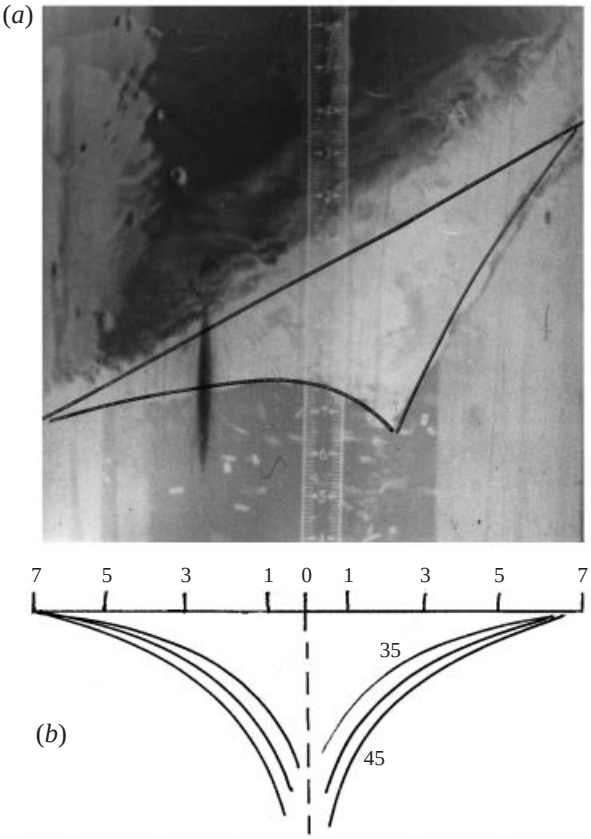

FIGURE 4. (*a*) A 16 mm ciné photograph of a turbulent rotillation wave and the resultant vortex. The vortex was filmed from the side, and the edges of the figure are the sidewalls of the cylinder. A centimetre scale taped to the near wall of the cylinder appears at the centre. Other vertical streaks are light reflections from the Lucite cylinder. The straight slanted line indicates the approximate intersection of the water surface (the wave) with the cylinder wall. The wave height maximum is on the right and the wave trough is on the left. The curved lines indicate the intersection of the water surface with an imaginary plane through the centre of the vortex. The centre of the vortex lies about 2 cm off-axis toward the wave maximum and rotates with the wave. (*b*) The shape of the free surface for symmetrical constant-V vortices with $V = 35$, 40, and 45 cm s^{-1}. The radial scale is r (cm) and matches that of the cylinder above.

right. The vortex central depression is indicated with curved lines. These represent the intersection with the water surface of a vertical plane through the centre of the vortex. Despite some uncertainty in detail, the central depression of the vortex is clear with its centre about 2 cm off the cylinder axis. This centre wobbles with the frequency of the wave and thus has its average position on the axis of the cylinder.

Beneath the photograph are calculated shapes of the free surface for symmetrical vortices with $V = 35$, 40, and 45 cm s^{-1}. The observed vortex depression clearly is of similar shape relative to the overall slope of the water surface (slanted line) and suggests a speed in the interval $35 < V < 45$ cm s^{-1}.

In this experiment the speed of the rotillation wave at the cylinder wall was $V_W = \sigma R = 162.9$ cm s^{-1} compared to the approximate vortex speed $V \approx 40$ cm s^{-1}, about 25% of V_W. In the experiment of figure 2 the computed vortex speed was $V_o = 12.0$ cm s^{-1}, only 10% of the rim wave speed $V_W = 119.5$ cm s^{-1}.

FIGURE 5. An example of streaks from the spin-down experiment at $t = 90$ s. The exposure time of the camera shutter was calibrated to be $0.961\,\text{s} \pm 0.013\,\text{s}$. Although this long shutter time gave overlapping streaks at 90 s it was necessary to assure reasonable accuracy with the shorter streaks at later times.

4. Decay of a constant-ω vortex with a turbulent boundary layer

Starting from constant ω, but with a turbulent boundary layer rather than the laminar Bödewadt case, one should expect ω to decay more rapidly at the larger radii where the Reynolds number is larger. Thus a vortex initially having $\partial\omega/\partial r = 0$ should tend toward $\partial V/\partial r = 0$, and because such a state is stable for vortex decay it is postulated that any vortex of suitable size over a smooth stationary boundary should approach $\partial V/\partial r = 0$. For the experiment that follows it will be seen that R is too small and the time too short to produce a reasonable region of constant V, although a trend in that direction is apparent.

In a spin-down experiment with $\omega_o = 1.5\,\text{s}^{-1}$, $R = 15.24$ cm and $H = 21.7$ cm, streak photographs were analysed at 90, 120, 150, 180, 210, 240, 270 and 300 s. The steady spin down of the cylinder to rest took 30 s. Figure 5 shows a photograph of paper-dot tracers taken with an exposure time of 0.96 s, 90 s after the start of spin down. The streaks of figure 5 illustrate some of the problems of streak-velocity measurements: overlapping streaks if long streaks are desired and poor data coverage. A long exposure time (≈ 1 s) was necessary to obtain streaks of measurable length at the later stages of decay. The vortex was not perfectly symmetrical, especially from about 9 cm to the rim where the centrifugally unstable shear and the turbulent boundary layer caused large speed fluctuations. But about 100 or more streaks from each photo could be reliably measured and figure 6 gives examples of data at $t = 120$, 210 and 300 s. By 300 s the scatter from a smooth curve was largely due to observational error in the measurement of streak lengths, about 0.1 cm in length or $0.1\,\text{cm}\,\text{s}^{-1}$ in velocity.

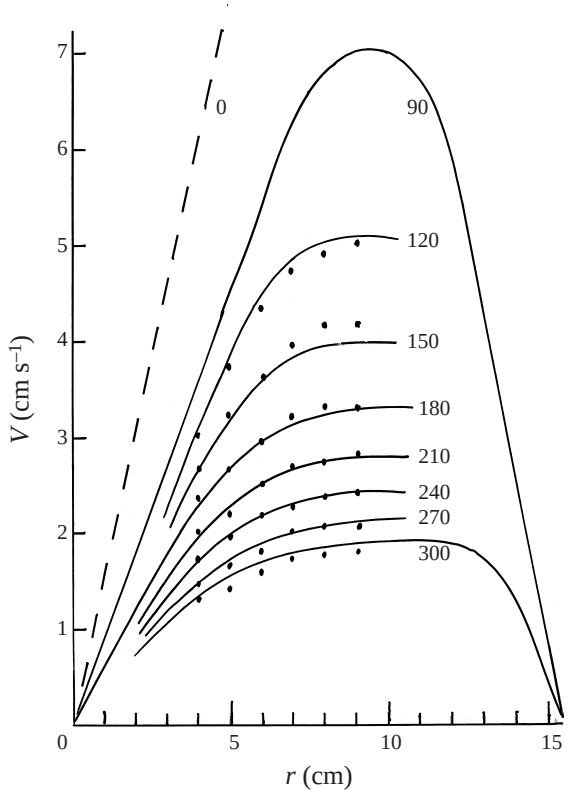

FIGURE 6. Spin down of a vortex started from $\omega_o = 1.5\,\mathrm{s}^{-1}$. The curves are from the numerical model with $A = 0.0708$, $B = -0.00085$. Plotted points are smoothed data at radii from 4 to 9 cm. The straight dashed line gives $V(r)$ at $t = 0$.

For an appropriate model of vortex decay start with the Navier–Stokes equation for $V(r, z, t)$ in polar coordinates, assuming circular symmetry (e.g. Schlichting 1960),

$$\frac{\partial v}{\partial t} + u\frac{\partial v}{\partial r} + w\frac{\partial v}{\partial z} + \frac{uv}{r} = \nu\left(\frac{\partial^2 v}{\partial r^2} + \frac{\partial (v/r)}{\partial r} + \frac{\partial^2 v}{\partial z^2}\right). \tag{18}$$

For the interior flow: $v \to V$, $u \to U$, $\partial V/\partial z = 0$, and (18) reduces to

$$\frac{\partial V}{\partial t} + U\left(\frac{\partial V}{\partial r} + \frac{V}{r}\right) = \nu\left(\frac{\partial^2 V}{\partial r^2} + \frac{\partial (V/r)}{\partial r}\right). \tag{19}$$

If the viscous terms are set to zero (19) is equivalent to the conservation of angular momentum, as asserted in § 2.

As before we represent the turbulent boundary-layer transport as $T_{B,t} = C^* V D_B/2$, but now C^* should be not only a linear function of Re, as derived for the constant-V case, but also some dimensionless function of $\partial V/\partial r$ as

$$C^* = ARe + B\, f(K\, \partial V/\partial r). \tag{20}$$

Higher derivatives of V also may be significant in certain cases. In (20) the coefficient K, the functional form $f(\,)$, and the constants A and B must be determined empirically, although A should have the same value as found in the constant-V case.

K must have the dimensions of time and should be composed of some combination

of the variates V, r, D_B and the fixed parameters ν, R and H. But of these we can rule out H and R if these are sufficiently large because then the transport should not depend upon either. And if we retain V, r, and ν, D_B is ruled out, D_B being the combination $D_B = (r\nu/V)^{1/2}$. Still, there are many combinations of V, r and ν that can have the dimensions of t such as $r/V, (r^3/V\nu)^{1/2}$, etc. Initial tests comparing a numerical model with data from the experiment using several combinations that included V in K, such as the two cited above, gave poorer results in comparison with $K = r^2/\nu$, the only possible combination that does not involve V. Thus the simplest representation of C^* in terms of $\partial V/\partial r$ with no additional factor involving V in the coefficient K appeared to be optimum.

Turning to the question of $f(\,)$ in (20), one can imagine many formulations such as $f(\,) = \ln(\,), (\,)^s$ etc. Once more anticipating the results, calculations with several trial forms of $f(\,)$ all gave inferior results to $f(K\partial V/\partial r) = (r^2/\nu)\partial V/\partial r$ when calculated profiles of $V(t)$ were fit to observed profiles. In particular, powers of $(K\partial V/\partial r)^s$ that included $S = 1.1$ and $S = 0.9$ clearly showed that $S = 1.0$ gave the best results. Thus the simple form

$$C^* = ARe + B(r^2/\nu)\partial V/\partial r \tag{21}$$

appears to give good results, as may be seen below, but of course there are other possibilities.

Substituting $U = C^* V D_B/2$ as before, (20) becomes

$$\frac{\partial V}{\partial t} = -C^* \left(V\frac{D_B}{2H}\right)\left(\frac{\partial V}{\partial r} + \frac{V}{r}\right) + \nu\left(\frac{\partial^2 V}{\partial r^2} + \frac{\partial (V/r)}{\partial r}\right). \tag{22}$$

By using the constants ν and H to define dimensionless variates (asterisks) we may write: $V = V^*\nu/H$, $t = t^* H^2/\nu$, and $r = r^* H$. Then (22) may be conveniently represented in the non-dimensional form

$$\frac{\partial V^*}{\partial t^*} = -\tfrac{1}{2}C^*(V^* r^*)^{1/2}\left(\frac{\partial V^*}{\partial r^*} + \frac{V^*}{r^*}\right) + \frac{\partial^2 V^*}{\partial r^{*2}} + \partial\frac{(V^*/r^*)}{\partial r^*}, \tag{23}$$

where $C^* = ARe + B(r^{*2}\partial V^*/\partial r^* - V^*)$. The corresponding equation for the non-dimensional angular momentum, $M^* = V^* r^*$, is

$$\frac{\partial M^*}{\partial t} = -\tfrac{1}{2}C^*(M^{*1/2})\frac{\partial M^*}{\partial r^*} + \frac{\partial^2 M^*}{\partial r^{*2}} - \frac{1}{r^*}\frac{\partial M^*}{\partial r^*}, \tag{24}$$

Optimum values of A and B were found by integrations of (24) and comparisons with smoothed data from the streak analyses. For $\partial M^*/\partial r^* < 0$ (i.e. a negative gradient of the angular momentum, near the rim) the condition $\partial M^*/\partial r^* = 0$ was substituted to avoid computational instability. In any case, flow near the rim was unstable and no reasonable comparison of the model and the data could be expected there. Smoothed data at seven time levels and six values of r, at 1 cm intervals from $r = 4$ to 9 cm, were used (figure 6). Data beyond 9 cm were obviously affected by the rim, and at small r there were few reliable values.

Integration starting from $t = 0$, the start of spin down, was not appropriate because the theoretical model assumes a fully developed turbulent boundary layer with negligible transients. In the laboratory experiment, however, the boundary layer initially was stable and laminar, and significant transients must have occurred for more than the 30 s spin-down time of the cylinder. Therefore, the initial values of $V(r)$ for the computation were taken from a smooth curve (figure 6) drawn through data at $t = 90$ s.

The computations used many trial combinations of A and B, matching the data to the computed values, and that combination was found that minimized the Erms. In each case Erms was based upon the data from all seven time levels (120, 150, 180, 210, 240, 270 and 300 s) and the corresponding computed values at the equivalent computation times 30, 60, 90, 120, 150, 180 and 210 s.

Figure 6 displays the data points used for the evaluation of A and B. At $t = 90$ s the maximum V, 7.0 cm s^{-1}, occurred at $r = 9.6$ cm, but the maximum $M^* = 7439$ was further out at $r = 11.9$ cm. Apparently the instability beyond $r \approx 12$ cm had penetrated inward beyond maximum M^* to nearly $r = 9$ cm so only data for $r \leqslant 9$ cm were used for Erms. The best combination of A and B was found to be $A = 0.0708$, $B = -0.00085$ with Erms $= 0.0848$ cm s^{-1}. The curves of figure 6 correspond to these values.

A conceptual difficulty arises with the use of $K = r^2/v$, however, as can be seen for a flow with $\partial\omega/\partial r = 0\,(V/r = \partial V/\partial r = \omega)$. A reduction of (22), letting $v = 0$, shows that the A and B terms yield

$$\frac{\partial V}{\partial t} = -\left(AV^2 + BV^{5/2}\frac{r}{v^{1/2}}\right)/2H \quad (\partial\omega/\partial r = 0, K = r^2/v). \tag{25}$$

The term $-AV^2$ seems reasonable but the B term contains a higher power of V. Since B is negative, $\partial V/\partial t$ might become positive at large values of V. This would already be the case, for example, for $V = 10$ cm s^{-1}, $r = 4$ cm, $v = 0.01$ cm^2 s^{-1} ($Re = 63$) and $B = -0.00085$. A positive $\partial V/\partial t$ implies inward interior flow and outward boundary-layer transport which would seem to be physically unreasonable for a decaying vortex.

This higher power of V in (25) can be reduced by using $K = (r^3/Vv)^{1/2}$. Then for $\partial\omega/\partial r = 0$ the reduction of (22) leads to

$$\partial V/\partial t = -(A + B)\,V^2/H \quad (\partial\omega/\partial r = 0, K = (r^3/vV)^{1/2}), \tag{26}$$

where both A and B terms are now proportional to V^2. Note, also, that the A term in (26) is twice that in (14) and (25). This difference arises from the term $(\partial V/\partial r + V/r)$ which is simply V/r for (25) but $2V/r$ for (26). This effect represents a difference in the horizontal convergence due to the different distributions of radial inflow in the two cases.

The formulation $K = (r^3/Vv)^{1/2}$ was tested in the numerical model and led to $A = 0.069$ and $B = -0.035$ with Erms $= 0.1104$, significantly higher than with $K = r^2/v$. Which formulation of K is preferable? There is no firm basis for a decision, for there are other possible choices and the best formulation may change with the parameters of the problem. To accommodate a variable K by introducing a parameter p, a non-dimensional C^* may be written as

$$C^* = AM^{*1/2} + (B/M^{*p})(r^*\partial M^*/\partial r^* - M^*), \tag{27}$$

where the two cases above correspond to $p = 0$ and $p = 1/2$. It is certainly conceivable that the optimum p varies continuously with t and with r as $V(r)$ changes during spin down. But this is only one of many possibilities.

The discrepancies between the numerical calculation and the data at 120 and 150 s (figure 6) have more than one possible explanation. Most obvious would be inaccuracy of the data or inadequacy of the theoretical model. However, due to the abrupt initial deceleration and inward boundary-layer flow there are sizable oscillations, sometimes called 'elastoid-inertial' oscillations, in which rings of interior fluid oscillate in and out. By the conservation of angular momentum there are corresponding oscillations in V

and $T_{B,t}$, all of which damp out with time. Such oscillations are clearly visible when there is an abrupt deceleration of the tank to rest and are believed to be the principle source of the systematic discrepancies noted at 120 and 150 s and may have affected the initial curve at $t = 90$ s. Oscillations could not occur in the numerical model because they are not permitted by the simple first-order (in time) model equations that were developed and used. Oscillations in a model would require a time-dependent radial equation, an imbalance between U and $T_{B,t}$, and perturbations in height of the free surface.

The best result, $A = 0.0708$, is very close to $A = 0.072$ found for the constant-V vortex, thus supporting the theory that the leading term of C^* in such models should be $A\ Re$ with $A \approx 0.071$.

5. Stresses, torque, and the generation of a steady, constant-V vortex

5.1. *Torque and stresses*

In the derivation of (14), developed for only the interior flow, viscous stresses at the bottom were not explicitly included. Nevertheless their effect on the decay of the vortex was represented by radial convergence in the bottom boundary layer and, through continuity, the corresponding outward flow in the interior. Therefore the right-hand side of (14) represents the effect of this bottom stress at each value of r.

The rate of change of the angular momentum of the fluid at radius r equals the torque, $T_q(r)$, at the bottom boundary and is

$$T_{q,o}(r) = 2\pi r \int (\partial V/\partial t)\, \mathrm{d}z = -2\pi r A\, V^2/2. \tag{28}$$

Then the stress of the turbulent Bödewadt layer on the bottom boundary is

$$\tau_0(r) = A\, V^2/2. \tag{29}$$

5.2. *The initial, steady-state vortex and the required torque*

In the experiment of figures 2 and 3 the flow was not observed until 10 s after the stop of rotillation. Nevertheless, because $\partial V/\partial r = 0$ persisted it is presumed that this condition prevailed at $t = 0$, the stop of rotillation, and was the time-averaged flow during rotillation. This assumption is generally supported by the free surface shape of figure 4.

Although (28) was derived for a slowly decaying vortex, it also should apply well to a steady constant-V vortex. Then the negative torque of (28) must be balanced by a positive torque from the breaking/turbulent rotillation wave near $z = H$, $T_{q,H}(r)$. While there is little hope of theoretically deriving the magnitude of $T_{q,H}(r)$, the linear r dependence seems reasonable in view of the roughly linear dependence of the wave amplitude upon r. But it is also conceivable that within the turbulent wave there is a radial redistribution of $T_{q,H}(r)$ to satisfy conditions imposed by the interior flow and the bottom boundary layer.

While the concept of an adjustment of the source to satisfy interior and end conditions may at first seem bizarre, there is at least one published example (and perhaps others) in which this was precisely the case. In a source/sink experiment in a rotating basin (Faller 1960) water was withdrawn (the sink) from a vertical slot in the eastern boundary of a pie-shaped sector and was supplied from a western boundary current (the source). Interior geostrophic dynamics and Ekman boundary layer suction and pumping dictated a Gaussian lateral distribution of the flow from source to sink, the jet narrowing as it approached the sink. The interior and end

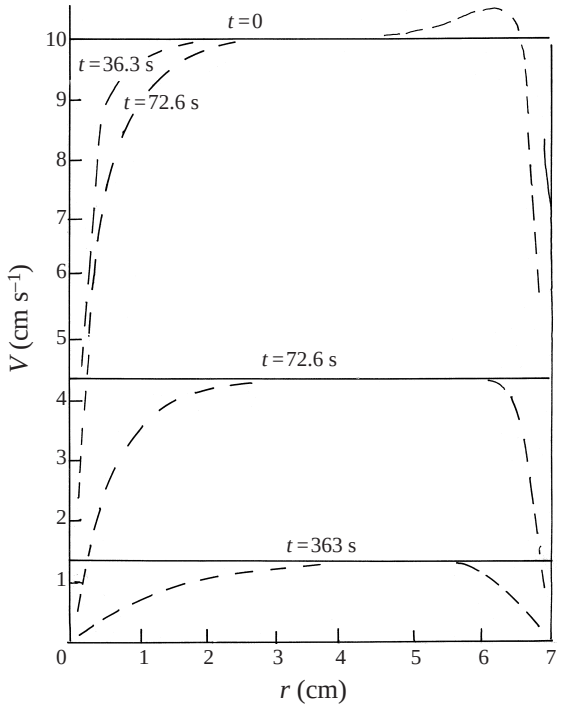

FIGURE 7. $V(r)$ from a numerical model based upon (30) starting from $V_o = 10\,\mathrm{cm\,s^{-1}}$. Solid lines are for $\nu = 0$ and dashed lines are for $\nu = 0.01\,\mathrm{cm^2\,s^{-1}}$. Top curves are for $S^* = 1.42 \times 10^7$ and lower curves show the decay with $S^* = 0$.

constraints required that the source water at the western boundary spread out to a Gaussian lateral distribution with a width proportional to the square root of the distance from the source to the sink. Thus it is speculated that in the present problem the primary radial distribution of torque provided by the breaking wave may not have been linear with r but may have been redistributed by the turbulence to satisfy the requirement of a constant-V vortex.

5.3. *Lateral viscous effects*

To numerically test the importance of lateral viscous effects in a case initially with $\partial V/\partial r = 0$ but maintained by a torque, (24) was modified by the addition of a non-dimensional source of angular momentum per unit mass

$$S^* = AV^2H^2/2\nu^2$$

to give

$$\frac{\partial M^*}{\partial t^*} = -\tfrac{1}{2}C^*(M^*)^{1/2}\frac{\partial M^*}{\partial r^*} + \frac{\partial^2 M^*}{\partial r^{*2}} - \frac{1}{r^*}\left(\frac{\partial M^*}{\partial r^*}\right) + S^*r^*. \tag{30}$$

Figure 7 shows $V(r)$ for integrations of (30) starting with $V_o = 10\,\mathrm{cm\,s^{-1}}$, $H = 20\,\mathrm{cm}$, $R = 7\,\mathrm{cm}$, $\nu = 0.01\,\mathrm{cm^2\,s^{-1}}$ or 0, $A = 0.071$, and $B = -0.00085$. First considering the case $\nu = 0$, the end conditions were $\partial V/\partial r = 0$ at $r = 0$ and at $r = R$. Then the source required to maintain $V = 10\,\mathrm{cm\,s^{-1}}$ at all r was $S^* = 1.42 \times 10^7$, exactly the value required from theory. With $S^* = 0$ the flow decayed as shown by the solid horizontal lines at 72.6 s and 363 s.

With lateral viscous effects (dashed lines) and the end conditions $V = 0$ at $r = 0$

and at $r = R$, the flow decayed rapidly at small r but soon approached the steady state shown for $t = 72.6$ s. Nevertheless $V \approx 10\,\mathrm{cm\,s^{-1}}$ was maintained over a large range of r. (The hump in V toward the rim was caused by the substitution of $\partial M^*/\partial r^* = 0$ for $\partial M^*/\partial r^* < 0$ (near the rim) needed to avoid computational instability.) In reality of course the turbulent rim boundary layer would be much wider than in the computations. These computations confirm that a continuous source S^* can generate a steady interior flow with $\partial V/\partial r = 0$ as appears to have been the case for the rotillation experiments.

6. Conclusions

The following conclusions are at present restricted to and refer to symmetric vortices in relatively deep liquids over smooth, stationary boundaries and with turbulent Bödewadt boundary layers having $Re < 100$. The vortices must be large enough that interior lateral viscous effects are negligible and side boundary layers are remote.

(i) In addition to other special vortices such as the Vr vortex, $\partial M/\partial r = 0$ and the constant angular velocity vortex, $\partial\omega/\partial r = 0$, we may add the constant-V vortex, $\partial V/\partial r = 0$. Such a vortex has been measured in rotillation experiments from streak photographs of the free surface and is supported by an observation of the shape of the free surface in a similar case with more extreme turbulence.

(ii) During decay such a vortex maintains $\partial V/\partial r = 0$, i.e. $\partial(\partial V/\partial r)/\partial t = 0$. This condition leads directly to the specific result that a dimensionless factor, C^*, that characterizes the turbulent radial boundary-layer transport must be given by $C^* = A\,Re$, where $Re = V\,D_B/\nu = (Vr/\nu)^{1/2} = r/D_B$. From the experimental data $A \approx 0.072$.

(iii) From a numerical model and related theory, a constant-V vortex will occur in a steady state when there is a continuous source of angular momentum that is proportional to radius.

(iv) The radial boundary-layer transport (per unit length of circumference) in a constant-V vortex is given by $T_{B,o} = C^* V\,D_B/2 = A(Re/2)(Vr\nu)^{1/2} = A\,Vr/2 = AM/2$. Thus the transport is proportional to the local angular momentum. The stress of the fluid on the boundary is $\tau_o = \rho A\,V^2/2$.

(v) For a vortex with $\partial V/\partial r \neq 0$ the radial transport and stress may be found by using $C^* = ARe + B(r^2/\nu)\partial V/\partial r$. The best fit to the experiment, started from solid rotation, gave $A = 0.0708$, $B = -0.00085$. But this formula and the associated value of B are uncertain and may well vary with $V(r)$ and its derivatives. The value $A \approx 0.071$ seems relatively secure, however, since two quite different experiments gave nearly the same value.

Extensions of these results to higher Re, rough surfaces and rotating systems are quite practical. With boundary roughness an additional parameter such as z_o/D_B, where z_o is a roughness length, would appear. Since the experiments involve only the measurement of $V(r)$, $\partial V/\partial r$ and the rate of decay, the same general procedure could be used in steadily rotating systems where the ratio ω/Ω, a Rossby number, would be an additional parameter. Detailed numerical models to test the turbulent boundary-layer transport relations at low Reynolds numbers would be valuable but must include curvature and $\partial V/\partial r$, and must span a sufficient range of r to account for the horizontal and vertical convection of turbulence inherent in such flows.

These results for turbulent boundary-layer transport are not necessarily restricted to symmetrical vortices but may be applicable in more general problems of curved flow. Perhaps the most restrictive condition will be that transients in the free-stream flow should be small.

The author is indebted to Dr John Whitehead at the Woods Hole Oceanographic Institution for the use of its fluid dynamics laboratory for the recent vortex decay study and for the rotillation experiments conducted during a sabbatical year from the University of Maryland, 1977–78. The early research on rotillation was supported in part by the National Science Foundation under Grant ATM 76-82051.

REFERENCES

Bödewadt, U. T. 1940 Die Drehstromung über festem Grunde. *Z. Angew. Math. Mech.* **20**, 241.

Ekman, V. W. 1905 On the influence of the earth's rotation on ocean currents. *Archive. Math. Astron. Phys.* **2**, 11.

Faller, A. J. 1960 Further examples of stationary planetary flow patterns in bounded basins. *Tellus* **12**, 159–171.

Faller, A. J. 1991 Instability and transition of disturbed flow over a rotating disk. *J. Fluid Mech.* **230**, 245–269.

Greenspan, H. P. & Howard, L. N. 1963 On a time dependent motion of a rotating fluid. *J. Fluid Mech.* **17**, 385–404.

Lingwood, J. R. 1997 Absolute instability of the Ekman layer and related rotating flows. *J. Fluid Mech.* **331**, 405–428.

Maas, L. R. M. 1993 Nonlinear and free-surface effects on the spin-down of barotropic axisymmetric vortices. *J. Fluid Mech.* **246**, 117–141.

Pikhtov, S. V. & Smirnov, E. M. 1992 Boundary layer stability on a rotating disk with corotation of the surrounding fluid. *Izv. Akad. Nauk, SSSR Mek. Zhid. Gaza* **27**(5), 69–77.

Prandtl, L. 1949 Erzeugung von Zirkulationen beim Schutten von Gefassen. *Z. Angew. Math. Mech.* **29**, 8–9.

Savas, Ö. 1987 Stability of Bödewadt flow. *J. Fluid Mech.* **183**, 77–94.

Schlichting, H. 1960 *Boundary Layer Theory*. McGraw-Hill, 647 pp.

Stern, M. E. 1960 Instability of Ekman flow at large Taylor number. *Tellus* **12**, 399–417.